Computer-aided diagnosis system of lung carcinoma using Convolutional Neural Networks

Fangjian Han
Lensee Bio-Technology Co.Ltd.
Ningbo,China
hanfangjian@hotmail.com

Li Yu
Lensee Bio-Technology Co.Ltd.
Ningbo,China
22379006@qq.com

Yi Jiang
2nd Xiangya Hospital of Central South University,Changsha,China
jiangyi76@csu.edu.cn

Abstract

With the number of lung cancers' morbidity and mortality is showing a trend of increasing year by year, the demand for pathologists is increasing rapidly, so in this study, we aimed to design a medical pathologically assistant diagnostic system to help pathologists complete diagnostic analysis tasks. A Deep Convolutional Neural Network(DCNN) is adopted to automatically distinguish tumor tissues from normal tissues in digitized hematoxylin and eosin (H&E) stained lung cell pathological slides that collected from The Cancer Genome Atlas (TCGA) and collaborate hospitals, we trained and evaluate WSIs(the whole slide images) captured at 10x magnification and other higher magnification, results show the difference are negligible. Moreover, we also compared the training effect of different models on same level magnification WSIs, the results show that performance of Resnet-18 network model and Resnet-50 network model is nearly consistent. Actually processing time based on Resnet-18 model is shorter than Resnet-50 model, so we don't need deeper network for study. Our system was shown to enormous advantages in accuracy, sensitivity and efficiency, could reduce the burden on pathologists, enable them to spend more time on advanced decision-making tasks, would be widely applied to pathological diagnosis, clinical practice, scientific research and so on.

1. Introduction

Lung cancer is the most common cancer in the world and it is the leading cause of cancer-related death. Data shows, in 2018, 2.1 million new lung cancer cases and 1.8 million deaths from lung cancer [1]. A large number of lung cancer cases imply a sharp increase in the workload of diagnostic analysis. Currently, a range of issues, such as shortage of pathologists and long training cycle, time-consuming artificial pathological diagnosis, missed diagnosis, and misdiagnosis, urge the rapid development of digital pathology to serve the progress of practical pathological diagnosis and clinical diagnosis support.

In the past decade, the rapid improvement of computer processing capability, the progress in image analysis algorithm, and the rise and update of big data research methods have led to the development of computer-aided medical pathological data analysis technology[2-4]. Applying machine learning algorithm for cancer identification is proved to be efficient and accurate[5-16]. At present, the most widely application scenarios is breast cancer section identificated analysis[17-20], research on the identification of lung cancer has also been developing in recent years.

In recent years, lung cancer histopathological image identification has been developed. Nicolas Coudray, Paolo Santiago Ocampo, et al, used deep learning models to accurately classify WSIs into adenocarcinoma, squamous cell carcinoma, and normal lung tissue, and obtained better sensitivity and specificity. The average area under the curve (AUC) measured in the suffered population was about 0.97[21]. Xin Luo, et al. developed a pathological image analysis pipeline to automatically extract morphological features and build a statistical model based on these extracted features to predict the prognosis and survival outcomes of lung cancer patients. The results showed that algorithmic models for hematoxylin and eosin (H&E) stained lung cell pathological slides were objectively analyzed and successfully predicted the prognosis of patients with adenocarcinoma (ADC) and squamous cell carcinoma (SCC) [22]. In stage I lung cancers from the Cancer Genome Atlas (TCGA) dataset, Kun-Hsing Yu, Ce Zhang and Gerald J. Berry differentiate patients into short-term survivors and long-term survivors by using standardized machine learning methods to select the main features. The results show that automatically acquired image features can predict the prognosis of lung cancer patients, thus contributing to accurate oncology [23].

In this study, we proposed a lightweight, low-magnifying and high-efficient image recognition algorithm model. It

adopted Deep Convolutional Neural Network (DCNN) architecture to develop and evaluate, We collected a variety of lung tissue slides (including tumor slides and normal slides) from Cancer Genome Atlas (TCGA) and several cooperative medical institutions, digitally processed them into whole slide images (WSIs) at 10x magnification, 20x magnification and 40x magnification respectively, then these image data was fed into DCNN model for training, various performances were evaluated. The result showed that magnification level had little effect on the properties of the recognition model, while 10x magnification WSIs could save more memory space and processing time. In order to comparing different DCNN model's training effect, we evaluate the Relative operating characteristic(ROC) curve in Resnet-18 and Resnet-50 respectively, Resnet-18 in this paper shows better generalization performance. The following part of this paper will introduce in detail the experiment methods and results of model optimization and adjustment, as well as the summary of conclusions and insights for further researches.

2. Methods

2.1. Data collection

The model training method of deep learning network requires a large number of data sets to reduce the risk of overfitting. We obtained nearly 500 image data on the official website of the Cancer Genome Atlas (TCGA). However, this amount is not enough. To solve the problem of insufficient data, we collected 4500 pathological glass slides of H&E-stained lung tissues from collaborate hospitals, including Xiangya Hospital, the First Hospital of Changsha City and Hunan Cancer Hospital within two years(Nov 2017-Nov 2019).All the pathological glass slides were approved by each hospital and related research institutions. All patients that the study concerned had been well-informed. The images of glass slide of lung tissue were converted into digital whole slide images (WSIs) by using a multifunctional integrated digital slide scanner Professional pathologists labeled the cancerous area on site or remotely.

Datasets	Total	Type	Train	Validate	Test
TCGA	500	Tumor	245	52	53
		Normal	105	23	22
Collected	4500	Tumor	2100	450	450
		Normal	1050	225	225

Table 1: Detailed description of the datasets

2.2. Self-developed multifunctional integrated digital slide scanner

Similar to the general digital slide scanner, the multifunctional integrated digital slide scanner had the function of automatically scanning the pathological glass slides of lung tissues and converting them into WSIs. In addition, our scanner could divide the WSIs into small blocks during the conversion process. These small blocks were suitable for CNN without extra cutting of WSIs through open-slide tools, which greatly saved the processing time of the dataset.

2.3. Digital image data

All the whole slide images were captured at 10x magnification. The glass slide samples selected by the study were representative, including as many types of lung cancer as possible. We also included sections containing artifacts, such as bubbles, irregular micro-section knife sections, fixation problems, cauterization, folds, cracks, stripes and fuzzy areas, etc. The training samples containd as many different situations as possible, which improved the generalization ability of the training model.

2.4. Data labeling and the self-developed medical pathological assistant diagnostic system

We developed self-developed medical pathological assistant diagnostic system (Lensee Bio-Technology Co.Ltd.,Ningbo, China. https://www.sectormute.cn/lanxi/). Four part-time experienced pathologists labeled the image data in our system. We included 1650 normal lung tissue sections and 3350 lung cancer tissue sections. We selected 70% of the two categories of data as the training dataset, 15% as the validation dataset and 15% as the test dataset. We used the training dataset and validation dataset for hyper-parameter tuning and model selection. We used the test dataset to estimate the generalization performance of the final model .

2.5. Data Handling and Storage

The size of the WSI was large. One WSI (captured at 10x magnification) typically consumed 2-3 Gb of memory up to 10 billion pixels, which was not conductive to model analysis. Typically, the entire image was cut into 256 ×256 blocks as input data for the deep learning model. In this study, our self-developed multifunctional integrated digital slide scanner automatically cut the WSIs into 256×256 small blocks, which saved a lot of image processing time. Generally, a complete WSI could be divided into 10,000-15000 blocks. For training and validation, we removed the blank blocks that only contained the background area. According to the pathologists' label, we marked the "cancerous" or "non-cancerous" icon for each block. To improve the efficiency of the training model, we scrambled all the image blocks in the training dataset. If one block is cancerous, it must contain at least one cancerous lesion. Conversely, if one block is non-cancerous, it must not contain any cancerous lesion. For the data in the test

dataset, we did not need to mix all the WSI blocks together. We just input the blocks of each WSI into the model together to test whether the results meet the expected.

2.6. Algorithm framework DCNN

The DCNN network architecture used for training in this paper is the ResNet network architecture. Residual learning explicitly reconfigured the layer as the reference layer input to learn the residual function rather than the function that was not referenced. Previous studies had shown that the residual network was easier to optimize, and the accuracy could be gained by increasing the depth, that was, the layers behind the deep network can realize the identity mapping to solve the network degradation problem. The residual network was several orders of magnitude more complex than the same depth VGG networks [24], simplifying the network structure.

$$y = F(x, \{W_i\}) + x \quad (1)$$

Here x and y were the input and output vectors of the considered layers, respectively. The function $F(x, \{W_i\})$ represented the residual mapping to be learned. For the example of the two layers of a building block of residual learning model in Figure 1, $F = W_2\sigma(W_1 x)$,where σ represented ReLU . The shortcut section here did not introduce additional parameters or computational complexity, and the dimensions of x and F must be equal in equation (1).

If the dimensions of the x and F transforms were not equal, a linear projection W_S could be executed through the shortcut to match the dimensions:

$$y = F(x, \{W_i\}) + W_S x \quad (2)$$

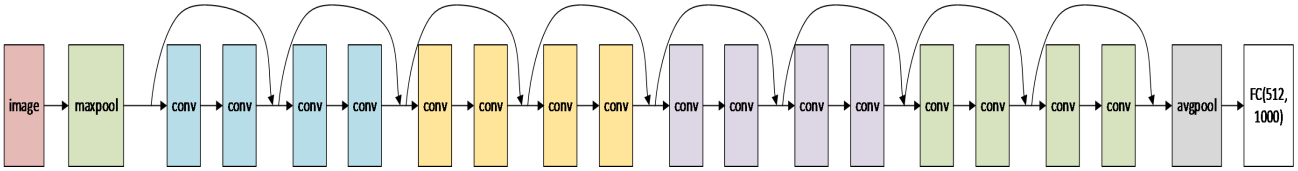

Figure 1: Framework diagram of ResNet-18 model

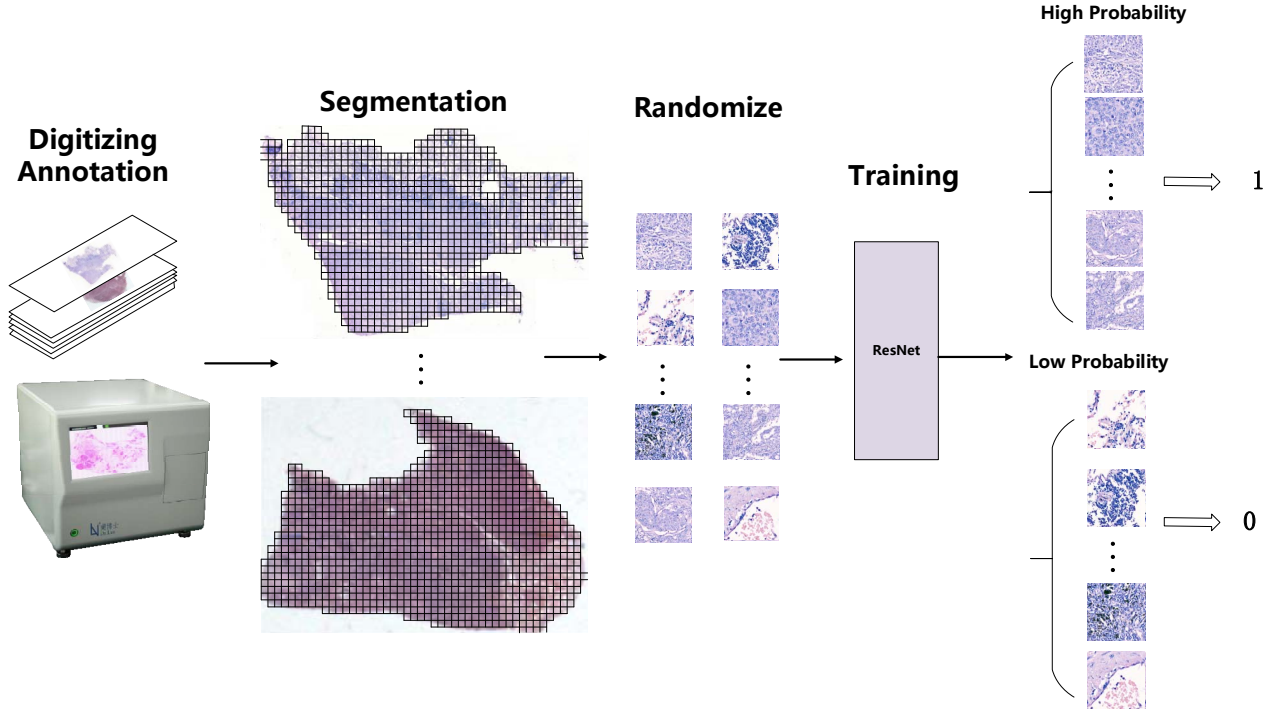

Figure 2: Flow chart for training model.

The structure of the ResNet-18 network in this paper was shown in Figure 1. Each building block for each stack layer follows the mapping transformation as follow.

The residual function F , was flexible in form and could represent monolayer or multilayer. The function

$F(x,\{W_i\})$ could represent multiple convolutional layers and perform element addition one by one on the channel basis of two feature maps.

2.7. Hardware platform

Since the training ability and efficiency of CNN model largely depended on the computing power and memory capacity of the computer, so we used a higher-configured computer to train our model. This computer had two 16-core 3.2GHz processors and two RTX2080Ti graphics processor units. For the practical use of scanning and diagnosis, we deployed the trained model algorithm on ARM Cortex-A57 (quda-core).

2.8. Model training

We completed our training process in a high-powered hardware platform. The training tool was PyTorch and the network architecture is ResNet. Model training process is shown in Figure 2. The original block of 256×256 size was cropped. Generally, we only removed the edge part, leaving the middle part. Therefore, the training scale of each block is 224×224. The initialization of network weights was important because poor initialization might lead to learning pauses due to gradient instability in deep networks [20]. To solve this problem, we used a random initialization method to configure the weight parameters. Similarly, we enhanced or corrected the input image by adjusting parameters such as brightness, contrast, saturation, and hue. Moreover, We implemented a random dithering process to enhance the randomness of the training dataset In this study, there were about 6000 million slicing samples in the training dataset. On our deep learning hardware platform, the individual training time was less than 30 minutes. We iterated the entire training process for about 100 times depending on repeated training and back propagation. It took 1-2 weeks to train These network.

3. Results

3.1. Accuracy of algorithms and models

We used the test dataset to evaluate and test the trained algorithm model. As mentioned in the method part, the blocks in the test dataset were not shuffled to facilitate the statistics on the accuracy of each pulmonary histopathology glass slide, the performance of accuracy and sensitivity in this algorithm model is shown in Figure 3. We can directly evaluate and compare the results identified by algorithm to the same WSI as the pathologist's annotations. We showed a comparison of the model test results with the ground-truth annotations in Figure 4.

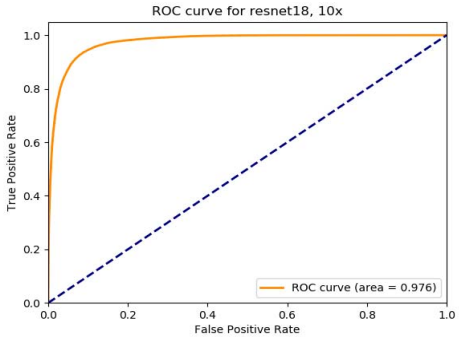

Figure 3: ROC curve representing the performance of ResNet-18 network in this paper

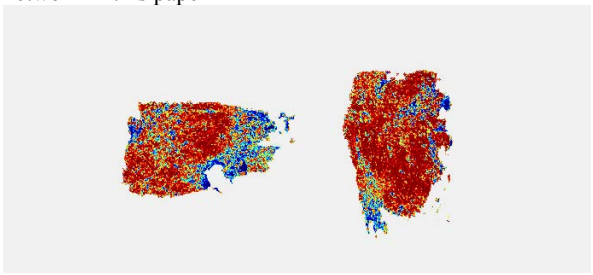

Figure 4a: AI model predicted result

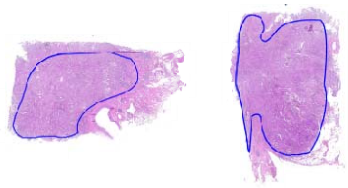

Figure 4b: ground-truth results by pathologist
Figure 4: Comparison of the model test results with the ground-truth annotations

3.2. Impact of image magnification on model efficiency

Unlike the 20x and 40x magnification images collected in previous studies, our training samples were collected at a 10x magnification. To prove that the effect of reduced magnification on model training was negligible, we scanned the same batch of slices and digitized them into 40x and 20x WSIs with the same process mentioned above. Then, the blocks were sent to the ResNet-18 model for training. After training, we finally evaluated the performance of the model in the test set. Figure 5 showed the test results, we can see the Area Under Curve(AUC) based on model is 0.976 at 10x magnification,0.996 at 20x magnification and 0.999 at 40x magnification. The performance of the trained high-magnification sampled images did not improve significantly. Both of the processing time and memory usage of 10x magnification WSIs were one-sixteenth of 40x image, greatly improved work efficiency, and which

verified the advantage of using 10x objective sampling slice images in this study.

3.3. Efficiency of the ResNet-18 network compared to ResNet-50 network

We also used the same training dataset to train in a ResNet-50 network, and measured the performance of the model trained on the same test dataset at 40× magnification. Figure 5 showed the learning characteristic curves trained under the two algorithm models, the Area Under Curve(AUC) respectively 0.999 of ResNet-18 model and 0.998 of ResNet-50 model. The AUC of the ResNet-18 network was slightly larger than that of the ResNet-50 network, Additionally training time and testing time based on Resnet-18 model is half of Resnet-50 model, so Resnet-18 network is enough for this research.

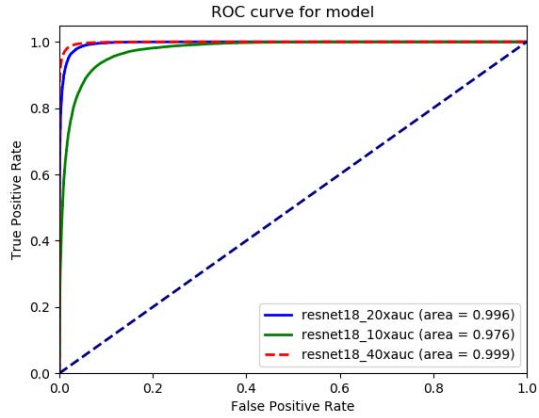

Figure 5: ROC curves of same test set with 40x magnification based on ResNet-18 and ResNet-50, and ROC curves of image data set with different magnification on ResNet-18 framework

3.4. Efficiency of the medical pathological assistant diagnostic system

When we used the trained model in the medical pathological assistant diagnostic system, the histopathology images on normal pathological slide (15×15mm) were identified for less than one minute. The assistant system could quickly locate the highly suspected lesion area and display the area on the interface to facilitate the pathologist's examination for further diagnose. In addition, the recognition program of trained model did not require strong computing power and huge memory capacity to support. It can work on an ARM core processor with 8GB of memory after experiments. As shown in Figure 6, a complete slice digitization and identification process will last about 60 seconds. The memory occupied by the system in the process of slice scanning and image stitching is not large, and a large amount of operating memory will be occupied when AI tumor discrimination is conducted, but it is not beyond the normal range of CPU.

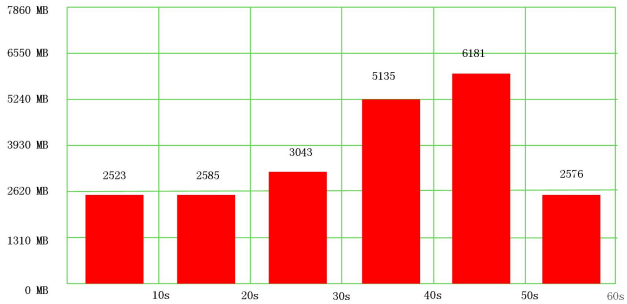

Figure 6: Host memory usage when the system is running

4. Conclusion

This paper presented the application of convolutional neural networks in the field of histopathology of lung cancer to improve diagnostic efficiency and reduce the workload of pathologists. The final deep learning framework we used in this paper was ResNet-18. For the lack of publicly available tissue slide sample data for lung cancer, we additionally collected 5000 different kinds of lung tissues slides from cooperative hospitals for training and testing. The final test results showed that the application of the ResNet-18 network model in the field of lung cancer recognition was effective and stable, and compared to Resnet-50, performance of ResNet-18 network is nearly similar. Actually processing time based on Resnet-18 model is shorter than Resnet-50 model, so we don't need deeper network for study.

The digital WSIs in this study were all at 10x magnification. Therefore, the training model was suitable for digital images collected with low magnification, and could quickly and accurately shows the prediction results. By comparing with 20x and 40x WSIs, the accuracy and the sensitivity of the results after training with our low-magnification WSIs has not decreased significantly, as well as the average AUC was suitable for the preliminary lung cancer diagnostic scenario.

We ultimately deployed the trained model on an TX2-based digital slide scanner that enabled diagnostic functions in combination with the scanning process to achieve functional integration, as well as remote access to WSIs by logging into the medical pathology-assisted diagnosis system. To test the generalization ability of the model, we deployed our system in the hospital. After a long period of practice, it had been proved that the auxiliary diagnosis system of lung cancer had certain practicability and accuracy in clinical diagnosis.

References

[1] F. Bray, J. Ferlay, I. Soerjomataram, R.L. Siegel, L.A. Torre, A. Jemal, Global cancer statistics 2018: GLOBOCAN estimates of incidence and mortality worldwide for 36 cancers in 185 countries. CA Cancer J Clin 68 (2018) 394-424.

[2] L. Pantanowitz, Digital images and the future of digital pathology. J Pathol Inform 1 (2010).
[3] A. Madabhushi, Digital pathology image analysis: opportunities and challenges. Imaging Med 1 (2009) 7-10.
[4] J.M. Prewitt, M.L. Mendelsohn, The analysis of cell images. Ann N Y Acad Sci 128 (1966) 1035-1053.
[5] A. Fourcade, R.H. Khonsari, Deep learning in medical image analysis: A third eye for doctors. J Stomatol Oral Maxillofac Surg 120 (2019) 279-288.
[6] Z.A. Simonyan K Very Deep Convolutional Networks for Large-Scale Image Recognition. Computer Science (2014).
[7] K. Bera, K.A. Schalper, D.L. Rimm, V. Velcheti, A. Madabhushi, Artificial intelligence in digital pathology - new tools for diagnosis and precision oncology. Nat Rev Clin Oncol 16 (2019) 703-715.
[8] D. Komura, S. Ishikawa, Machine Learning Methods for Histopathological Image Analysis. Comput Struct Biotechnol J 16 (2018) 34-42.
[9] H. Bisgin, T. Bera, H. Ding, H.G. Semey, L. Wu, Z. Liu, A.E. Barnes, D.A. Langley, M. Pava-Ripoll, H.J. Vyas, W. Tong, J. Xu, Comparing SVM and ANN based Machine Learning Methods for Species Identification of Food Contaminating Beetles. Sci Rep 8 (2018) 6532.
[10] S.I. Krizhevsky A, Hinton GE, ImageNet classification with deep convolutional neural networks. Adv. Neural Inf. Process. Syst. 25. Curran Associates, Inc. (2012) 9.
[11] G. Litjens, T. Kooi, B.E. Bejnordi, A.A.A. Setio, F. Ciompi, M. Ghafoorian, J. van der Laak, B. van Ginneken, C.I. Sanchez, A survey on deep learning in medical image analysis. Med Image Anal 42 (2017) 60-88.
[12] K. Fukushima, Neocognitron: a self organizing neural network model for a mechanism of pattern recognition unaffected by shift in position. Biol Cybern 36 (1980) 193-202.
[13] S.B. Lo, S.A. Lou, J.S. Lin, M.T. Freedman, M.V. Chien, S.K. Mun, Artificial convolution neural network techniques and applications for lung nodule detection. IEEE Trans Med Imaging 14 (1995) 711-718.
[14] S. Fiori, Riemannian-gradient-based learning on the complex matrix-hypersphere. IEEE Trans Neural Netw 22 (2011) 2132-2138.
[15] D.J. Russakovsky O , Su H, et al, ImageNet Large Scale Visual Recognition Challenge. International Journal of Computer Vision 115 (2015) 42.
[16] G. Campanella, M.G. Hanna, L. Geneslaw, A. Miraflor, V. Werneck Krauss Silva, K.J. Busam, E. Brogi, V.E. Reuter, D.S. Klimstra, T.J. Fuchs, Clinical-grade computational pathology using weakly supervised deep learning on whole slide images. Nat Med 25 (2019) 1301-1309.
[17] Spanhol F A, Oliveira L S, Petitjean C, et al. Breast cancer histopathological image classification using convolutional neural networks[C]//2016 international joint conference on neural networks (IJCNN). IEEE, 2016: 2560-2567.
[18] Shah M, Wang D, Rubadue C, et al. Deep learning assessment of tumor proliferation in breast cancer histological images[C]//2017 IEEE International Conference on Bioinformatics and Biomedicine (BIBM). IEEE, 2017: 600-603.
[19] Roux L, Racoceanu D, Loménie N, et al. Mitosis detection in breast cancer histological images An ICPR 2012 contest[J]. Journal of pathology informatics, 2013, 4.
[20] Apple S K. Sentinel lymph node in breast cancer: review article from a pathologist's point of view[J]. Journal of pathology and translational medicine, 2016, 50(2): 83.
[21] N. Coudray, P.S. Ocampo, T. Sakellaropoulos, N. Narula, M. Snuderl, D. Fenyo, A.L. Moreira, N. Razavian, A. Tsirigos, Classification and mutation prediction from non-small cell lung cancer histopathology images using deep learning. Nat Med 24 (2018) 1559-1567.
[22] X. Luo, X. Zang, L. Yang, J. Huang, F. Liang, J. Rodriguez-Canales, Wistuba, II, A. Gazdar, Y. Xie, G. Xiao, Comprehensive Computational Pathological Image Analysis Predicts Lung Cancer Prognosis. J Thorac Oncol 12 (2017) 501-509.
[23] K.H. Yu, C. Zhang, G.J. Berry, R.B. Altman, C. Re, D.L. Rubin, M. Snyder, Predicting non-small cell lung cancer prognosis by fully automated microscopic pathology image features. Nat Commun 7 (2016) 12474.
[24] He K, Zhang X, Ren S, et al. Deep residual learning for image recognition[C]//Proceedings of the IEEE conference on computer vision and pattern recognition. 2016: 770-778.